

Peridynamic Modelling of Cracking in TRISO Particles for High Temperature Reactors

T.A. Haynes^{1,2}, A. Battistini², A.J. Leide^{3,4},
D. Liu⁴, L. Jones^{2,5}, D. Shepherd⁵ & M.R. Wenman²*

¹ School of Engineering, University of East Anglia,
Norwich Research Park, Norwich, Norfolk, NR4 7TJ

² Department of Materials & Centre for Nuclear Engineering,
Imperial College London, Exhibition Road, London, SW7 2AZ

³ United Kingdom Atomic Energy Authority, Culham Science Centre,
Abingdon, Oxfordshire, OX14 3DB

⁴ School of Physics, HH Wills Physics Laboratory,
University of Bristol, Tyndall Avenue, Bristol, BS8 1TL

⁵ National Nuclear Laboratory (NNL), NNL Preston Laboratory,
Springfields Works, Salwick, Preston, Lancashire, PR4 0XJ

Abstract

A linear-elastic computer simulation (model) for a single particle of TRISO fuel has been built using a bond-based peridynamic technique implemented in the finite element code ‘Abaqus’. The model is able to consider the elastic and thermal strains in each layer of the particle and to simulate potential fracture both within and between layers. The 2D cylindrical model makes use of a plane stress approximation perpendicular to the plane modelled. The choice of plane stress was made by comparison of 2D and 3D finite element models. During an idealised ramp to normal operating power for a kernel of 0.267 W and a bulk fuel temperature of 1305 K, cracks initiate in the buffer near to the kernel-buffer interface and propagate towards the buffer-iPyC coating interface, but do not penetrate the iPyC and containment of the fission products is maintained. In extreme accident conditions, at around 600% power during a power ramp at 100% power per second, cracks were predicted to form on the kernel side of the kernel-buffer interface, opposite existing cracks in the buffer. These were predicted to then propagate slowly. The SiC coating was predicted to subsequently fail at a power of 940%, with cracks formed rapidly at the iPyC-SiC interface and propagating in both directions. These would overcome the containment to fission gas release offered by the SiC ‘pressure vessel’. The extremely high power at which failure was predicted indicates the potential safety benefits of the proposed high temperature reactor design based on TRISO fuel.

Keywords

high temperature reactors, Generation IV, peridynamics, cracks, TRISO, coated particle fuel

Highlights

- Initial irradiation-induced stresses in a TRISO coated fuel particle were simulated using a peridynamics model.
- Cracks formed in the buffer during the initial rise to power.
- Cracks formed in the fuel kernel at around 6 times full power.
- Cracks formed in the SiC ‘pressure vessel’ layer at around 9-10 times full power.

1 Background

Following a small number of accidents in which nuclear fuel has been severely damaged, there is a desire to move towards fuel cladding technology that is more inherently safe. A number of so-called accident tolerant fuels (ATF) have been proposed for current light water reactor (LWR) reactor designs. These include coated zirconium alloy claddings; FeCrAl claddings; novel pellet materials and SiC-SiC composite cladding [1-14]. Moving to the longer term, advanced technology fuels (also termed ATF) offer the possibility of not only enhanced safety, but the opportunity to move towards higher burnups. Small modular reactors (SMRs) built on a factory-based production line could offer reduced build times and hence financial risk prior to commencement of initial power supply. In addition, SMRs offer the potential for load-following capability as well as higher temperatures giving better thermodynamic efficiency and improved economics [15-24]. They also offer the opportunity for nuclear to move beyond merely providing a baseload generating capacity in the drive for 'net zero'. By providing high temperature heat, the reactors could supply district heating, heat for industrial uses, and heat for hydrogen co-generation [25].

One example of an advanced technology fuel is tristructural-isotropic (TRISO) particle fuel, a micrograph of which is shown in Figure 1. The TRISO particle consists of a uranium-based fuel kernel surrounded by four layers of materials designed to offer fission product retention and structural support [26] with a total diameter of around 1 mm. The fuel kernels have historically been formed of uranium dioxide (UO_2) [27] or uranium oxycarbide (UCO) [15, 28], although uranium nitride (UN) [22] has been suggested as a means of increasing the density of fissile material. The layers encasing the fuel kernel consist of: a porous buffer layer of carbon intended to absorb fission product recoil and accommodate dimensional change; an inner dense pyrolytic carbon (iPyC) layer; a SiC layer to provide strength and act as a barrier to gaseous and metallic fission products [16]; and, a dense outer pyrolytic carbon (oPyC) layer. The iPyC and oPyC layers, at around 90% theoretical density, act as a barrier to species migration and protect the SiC from chemical attack [23]. The three outer layers (iPyC-SiC-oPyC) are termed the TRISO coating [29]. The TRISO particles are then embedded into surrounding graphite / SiC matrix 'compacts' to provide moderation and structural integrity.

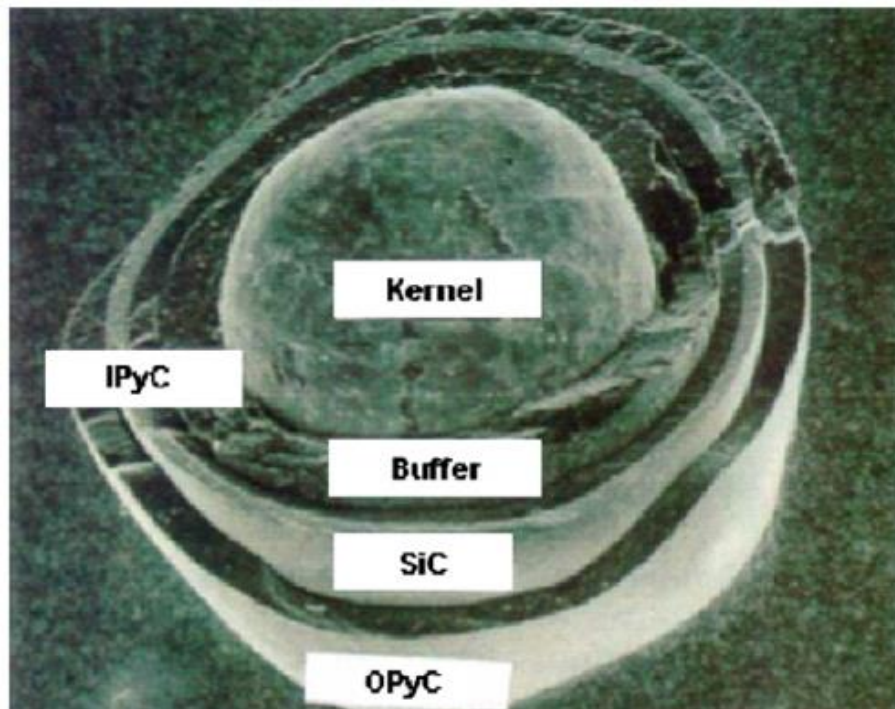


Figure 1 - A micrograph of a TRISO particle. Reproduced from Fig. 1 in [30].

Given that the SiC layer forms the primary barrier against fission product release, most models have been focused on this layer, frequently treating it as a pressure vessel. Li et al. considered the SiC as a rigid pressure vessel, perfectly bonded to the PyC layers [18]. A number of models have been developed that treat the carbon layers as visco-plastic and the SiC layer as purely elastic material [23]. The stress in the SiC is designed to be zero at the start of life. It then becomes compressive due to densification of the PyC layers, reaching the order of 100 MPa at a fast fluence of approximately $0.5 \times 10^{25} \text{ n m}^{-2}$ [23]. Due to PyC swelling and the build-up of carbon monoxide and dioxide (CO and CO₂), the stress increases towards the end of life. This has the potential to cause failure if it becomes tensile and greater than the fracture stress [23]. The historic approach is to assume spherical symmetry and solve the mechanics of the particle using closed form 1D analytical solutions [23]. This is analogous to conventional 2D(*r-z*) axisymmetric models for conventional pellet fuel in tubular cladding such as TRANSURANUS and ENIGMA [31, 32].

A more advanced finite-element approach is PARFUME (**particle fuel model**) [19, 33, 34]; it is analogous to ALCYONE, BISON or PELICAN [35-37]. Like PELICAN, PARFUME was built in the Abaqus finite element code and enables the modelling of a pre-imposed crack. The effect of a crack in the iPyC layer was to change the maximum principal stress in the SiC layer from a compressive stress of around 700 MPa (in the uncracked case) to a tensile stress of 440 MPa (in the cracked case) [33]. A further evolution is to analyse the statistical prediction of failure due to a number of interacting failure mechanisms which are computationally demanding to capture [38].

Techniques such as the extended finite element method (XFEM) require crack patterns to be imposed on a structure by the user. In contrast, peridynamics allows crack patterns to develop naturally. Phenomena such crack initiation, branching and retardation can be predicted as a result of the underlying geometry, material properties and loading. This paper investigates the behaviour of a TRISO fuel particle during early service life using a bond-based peridynamics

model implemented in Abaqus. This enables the prediction of the crack patterns within each layer, together with the interaction between cracks in each layer.

2 Methodology

2.1 Peridynamic Modelling in Abaqus

In peridynamics, objects are decomposed into a number of ‘material points’. The behaviour of each material point is dependent upon those in a horizon surrounding the material point, not just its nearest neighbours [39]. An example of this is shown Figure 2.

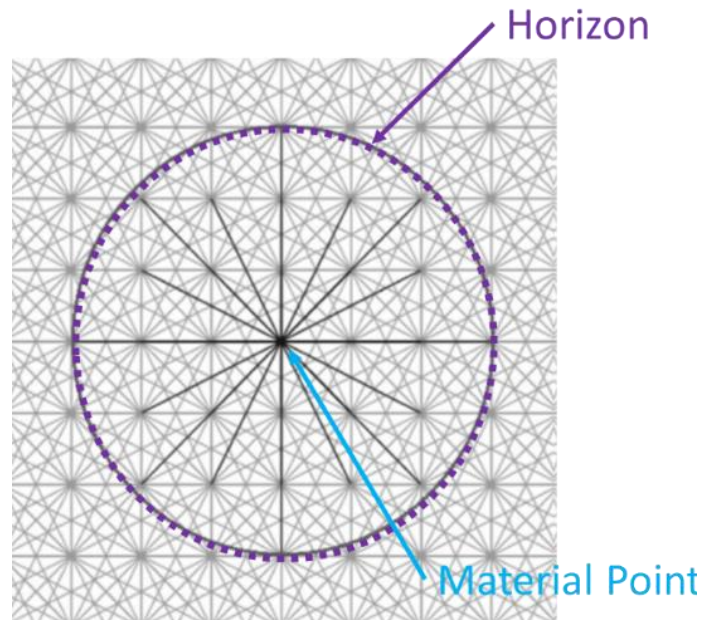


Figure 2 – A material point surrounded by a horizon of other material points. In bond-based peridynamics, bonds connect all of the material points within the horizon. Adapted from Figure 1 in [39].

‘State-based’ peridynamics uses information about the surrounding material points to determine the response of a material point. This approach has been applied by a number of authors [40], as well as to nuclear fuel more specifically [41-44]. ‘Bond-based’ peridynamics considers a number of bonds connecting a material point to surrounding material points. It can be readily introduced to a finite element code [39, 45-50] and the full range of material properties available in a finite element model employed. For this reason, a bond-based implementation of peridynamics in Abaqus was chosen for this work.

This work broadly follows the theoretical background, described by Le and Bobaru [51]. In the Abaqus implementation presented here, each ‘material point’ is represented by a node, and truss elements represent the ‘bonds’ linking the material points. This approach is discussed in more detail in [39].

Models Constructed

Two sets of peridynamic models were created and are presented in this work.

- A uniformly heated fuel kernel accompanied by an equivalent finite element model. These simulations were run to assess the appropriateness of approximating a spherical uniformly heated body as a disk in 2D and to verify the correct implementation of the material properties.
- The operation of isolated TRISO fuel particles under idealised conditions. These simulations are extended into a hypothetical fault. These consist of a linear increase in surface temperature to 1305 K over 24 hours, accompanied by a linear increase in kernel power to 0.267 W.

Uniformly Heated Fuel Kernel

Models of a uniformly heated 350 μm diameter fuel kernel were created using peridynamics and finite element analysis. Plane strain, plane stress and 3D finite element models were created with an element size of 7 μm . Two methods were employed to apply the power. The first was to apply a uniform volumetric heat flux; this could only be achieved in the finite element model. The second was to apply a temperature boundary condition to all of the material points, using the expression given by equation (17).

During a single 24-hour step, the temperature of the outside of the kernel was increased linearly from 293 K to 1305 K. This temperature was chosen to reflect the fuel volume averaged temperature in the AGR-2 experiment. During the same period, the volumetric thermal power was increased linearly to $1.19 \times 10^{10} \text{ W m}^{-3}$. This replicates that of Hu and Uddin [52] and is equivalent to a power of 0.267 W for a 175 μm radius kernel.

Spherical TRISO Particles

Figure 3 shows the model for TRISO particles used to investigate cracking during an idealised power history. Seventy rings of nodes were used across the radius of the particle, giving a nominal nodal separation of 5.6 μm . This gives a total of 15,373 nodes and 211,108 trusses at a horizon ratio of three. At the top, bottom, left and right of the model, the particle is constrained to not move in the azimuthal direction – this prevents spurious rotation. A temperature boundary condition is applied to the whole of the model and the temperature at individual nodes determined using the analytical solution described by equation (17).

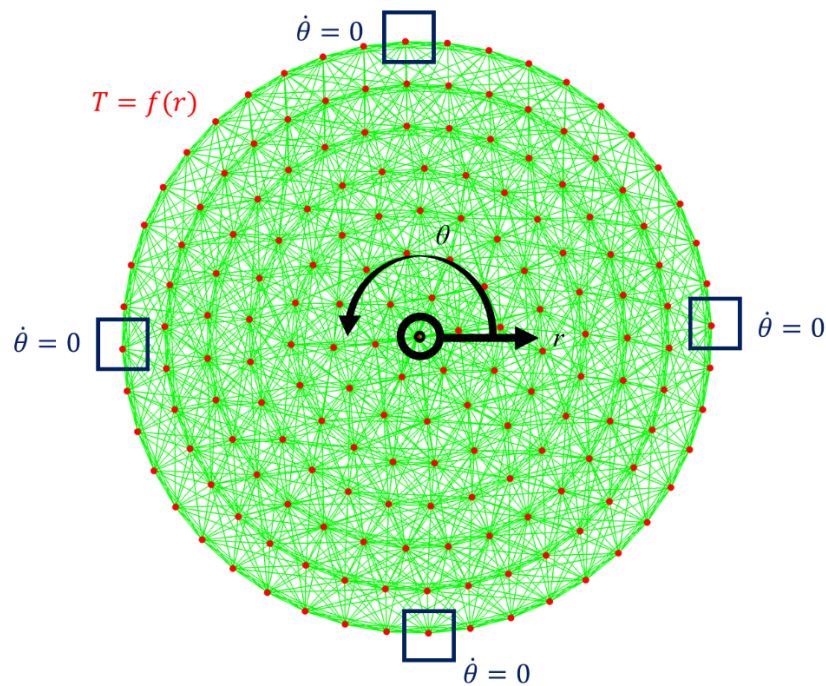


Figure 3 – Peridynamic model for TRISO particles used to investigate cracking during an idealised power history. For clarity, the nodal separation shown in this figure has been increased by a factor of 10.

The material properties of a bond depend upon the distance of the connected material points from the centre of the fuel kernel. Bonds which cross material interfaces are addressed in Section 2.3. The radius of each region of material are given in Table 1. The radius of each species was based upon a ‘standard’ particle with a 350 μm kernel diameter the layer thicknesses applied in the US AGR-1 and AGR-2 experiments [20].

Table 1 - The outer radius of each region of material of the TRISO fuel particles modelled.

	Thickness of Region (μm)	Outer Radius of Region (μm)
UO₂ Kernel	-	175
Buffer	100	275
iPyC	40	315
SiC	35	350
oPyC	40	390

2.2 Material Properties

The approach taken by this work was to use start of life material properties. This involved neglecting the impact of burnup and changes in porosity.

Porosity

The initial fractional porosities were assumed to be 0.010 for the UO₂ kernel; 0.560 for the buffer; 0.160 for iPyC ; 0.006 for SiC and 0.166 for oPyC [53].

Elastic Modulus

The elastic modulus of UO₂, E_{UO_2} , as described by MATPRO [54], is given by (1); the units for the elastic modulus are GPa; P is the fractional porosity and T the absolute temperature. It should be noted that these values were derived for conventional LWR fuel.

$$E_{UO_2} = 233.4(1 - 2.752P)(1 - 1.0915 \times 10^{-4}T) \quad (1)$$

The elastic modulus of the buffer, E_{BUF} , is given [55] by (2).

$$E_{BUF} = 34.5e^{-2.03P} \quad (2)$$

A number of expressions are available for the elastic modulus of PyC, E_{PyC} , [18, 55, 56]. The simplest, given in (3) and described by Park et al. [56], uses a standard correction term for porosity, originally derived for alumina [57], hence its representativeness of PyC is questionable and thus an area where new data should be sought. Further, it should be noted that this expression does not take into account the anisotropy of PyC; an alternative expression that includes the impact of this is available in [55].

$$E_{PyC} = 25.0(1 - 1.91P + 0.91P^2) \quad (3)$$

A number of correlations for the elastic modulus of SiC are available in the literature [58]. The relationship recommended by Powers [23], for use in TRISO fuel performance codes, is given by (4).

$$E_{SiC} = 460e^{-3.57P} - 0.04Te^{-962/T} \quad (4)$$

Poisson's Ratio

In bond-based peridynamics, Poisson's ratio is constrained to 1/3 in plane stress [59] and 1/4 in 3D [60] or plane strain [48]. Poisson's ratio was therefore constrained to 1/3 or 1/4, as appropriate in the peridynamics models. For the finite element models, the values given in Table 2 were used.

Table 2 – Poisson's ratio for each material in the finite element model

Material	Value	Source
UO ₂	0.32	[61-63]
Buffer	0.23	[55]
PyC	0.33	[18]
SiC	0.21	[58]

Thermal Conductivity

The thermal conductivity of nuclear materials is a function of their burnup, temperature, porosity and level of fission product contamination. A number of correlations for the thermal conductivity of UO₂ are available in the literature and have been discussed in depth elsewhere [64]. The starting point is normally setting the thermal conductivity of irradiated fuel to be the product of the thermal conductivity of unirradiated fuel, k_0 , and a number of correction factors. The thermal conductivity of unirradiated fuel [in J K⁻¹ m⁻¹] is usually expressed, using (5), as the sum of a phonon term, k_{ph} , [typically a power series in the absolute temperature, T] and an electronic term, k_{el} , [typically a negative exponential of the temperature].

$$k_0 = k_{ph} + k_{el} \quad (5)$$

Lucuta's model [65-67] is widely applied in the literature and so is given in more detail as an example. Lucuta's phonon and electronic terms, given by (6) and (7), are based upon the work of Harding & Martin [68].

$$k_{ph} = \frac{1}{3.75 \times 10^{-2} + 2.165 \times 10^{-4}T} \quad (6)$$

$$k_{el} = \frac{4.715 \times 10^9}{T^2} e^{-1.6361 \times 10^4/T} \quad (7)$$

A multiplicative porosity correction factor is given by (8), in which P is the fractional porosity and σ_s a shape function [set to 1.5 for spherical pores]. In this work, it was assumed that the fuel porosity was 1.0%.

$$K_P = \frac{1 - P}{1 + (\sigma_s - 1)P} \quad (8)$$

In the peridynamic models, the average thermal conductivity was determined in a user-defined sub-routine and used to determine the temperature profile in the kernel. More details on this approach are given in Section 2.4.

Thermal Expansion

Table 3 gives the coefficient of thermal expansion, α , assumed for each layer in the TRISO particle; all materials were assumed to be isotropic. In the peridynamics model, the total expansion of a truss is determined in the user-defined field subroutine and passed to Abaqus through a field variable. The code was amended to set the expansion as the average of that of the nodes at each end of the truss.

Table 3 – Coefficient of thermal expansion for each material.

Material	Value (K^{-1})	Source
UO ₂	1.0×10^{-5}	Williamson [69]
Buffer	3.5×10^{-6}	German & UK Data [55]
PyC	5.55×10^{-6}	Average of UK and German Data [55]
SiC	4.9×10^{-6}	Typical value at 1000 °C [24, 58]

Density

A volume-averaged density was determined to be $2.72 \times 10^3 \text{ kg m}^{-3}$ and this was applied to the models. Assigning an incorrect mass to nodes is not ideal. For instance, in the kernel the mass applied to each material point will be a third of that which it should be. Upon bond failure, elastic energy is converted into kinetic energy in the node. The velocity of the nodes will therefore be underestimated by a factor of $\sqrt{3}$. Work is ongoing to overcome this underestimate.

Fracture Stress

For a bond entirely within a material, i.e. not near a free surface or material interface, the fracture strength of the bond, $\sigma_{F,Bond}$, will be given by the fracture strength of that material. This is passed to Abaqus through the user-defined field sub-routine. The fracture stresses of each material, or pair of materials in the case of an interface are given in Table 4. The available data is sparse, consisting predominantly of strengths obtained at room temperature. The values used are given in Table 4. Of particular significance is that no data is available on the strength of either the kernel-buffer or buffer-PyC interface. In this work, we have set the strength of these two interfaces to be equal to the average of the materials on either side of the interface. Future work could investigate the appropriateness of this assumption against the backdrop of validation against experimental data.

Table 4 – Material fracture stresses assumed.

Material 1	Material 2	Strength (MPa)	Notes
Kernel	Kernel	150	Fracture strain [70], combined with room temperature elastic modulus
Kernel	Buffer	100	No data – average fracture stress of kernel and buffer used.
Buffer	Buffer	50	Based upon UK data for PyC and a correction for porosity [55]
Buffer	iPyC	150	No data – average fracture stress of buffer and iPyC used.
iPyC	iPyC	250	Average of US and German data in [55]
iPyC	SiC	870	Average of the normal and shear values obtained from TRISO particles [17]
SiC	SiC	620	Average of the values provided in [55]

SiC	oPyC	870	Average of the normal and shear values obtained from TRISO particles [17]
oPyC	oPyC	250	Average of US and German data [55]

2.3 Bonds Crossing Material Interfaces

For trusses crossing an interface, the assignment of material properties such as the elastic modulus to bonds is somewhat complicated. For example, the macroscopic elastic modulus differs at each end of the bond. In addition, one should bear in mind that the bonds or trusses are modelling constructs and do not exist. In contrast, the nodes represent the material surrounding themselves. The material exists and therefore the nodes have a physical meaning.

In this work, the strength of a truss crossing an interface is set to the assumed strength of the interface, given in Table 4. There are however several different ways of assigning an elastic modulus to the trusses. In this work, four approaches were considered:

1. Taking the average elastic modulus of the nodes at each end of the truss.
2. Modelling the truss itself as consisting of two materials with an interface at the midpoint of the truss.
3. Assuming the maximum elastic modulus of the nodes at each end of the truss.
4. Assuming the minimum elastic modulus of the nodes at each end of the truss.

By testing each approach, it was found that using the minimum elastic modulus of the nodes at either end of an interface truss gave the best overall behaviour for all of the interfaces. In addition, using the minimum stress would be sensible in the light of Weibull's weakest link theory for brittle fracture [46, 71, 72].

2.4 Thermal Model for a TRISO Fuel Particle

A temperature boundary condition was applied to all nodes using the user-defined displacement sub-routine. The temperature profile was based upon a simple pseudo-steady-state temperature solution. This relied upon the following two approximations:

- That all regions except for the kernel were held at the same bulk temperature. Effectively the kernel is embedded in an infinite thermal sink.
- The thermal conductivity of the kernel varied with temperature, as shown and discussed in Section 2.2. The thermal conductivity, averaged across all of the nodes in the kernel, k_{av} , was then determined. This was justified by the comparatively low temperature drop across the kernel.

The temperature assumed for bulk material was set to 1305 K at full power. This was based upon the fuel volume averaged temperature reported for AGR-2 [53].

The volumetric heat flux was taken from Hu and Uddin [52] and gives a power of 0.267 W (1.19×10^{10} W m⁻³) for a 350 μ m diameter kernel and agrees with the value of 0.3 W used by Rodríguez Garcia et al. [73].

Poisson's equation for heat flow in the presence of a volumetric heat flux in W m⁻³, q , is given by (9), in which k is the thermal conductivity in W m⁻¹ K⁻¹, T the temperature in K and ∇^2 the Laplace operator with units m⁻² [74].

$$\nabla^2 T = -\frac{q}{k} \quad (9)$$

Using spherical polar co-ordinates, assuming an average thermal conductivity, an isotropic heat flux and azimuthal symmetry transforms (9) into (10).

$$\frac{1}{r^2} \frac{d}{dr} \left(r^2 \frac{dT}{dr} \right) = -\frac{q}{k_{av}} \quad (10)$$

Integrating once gives (11).

$$r^2 \frac{dT}{dr} = -\frac{q}{3k_{av}} r^3 + A \quad (11)$$

At the origin ($r = 0$), the heat flux is a minimum in order to maintain symmetry. This necessitates setting the integration constant, A , to zero. Equation (11) therefore becomes (12).

$$\frac{dT}{dr} = -\frac{q}{3k_{av}} r \quad (12)$$

Integrating once more gives (13).

$$T = -\frac{q}{6k_{av}} r^2 + B \quad (13)$$

Substituting the outer radius of the kernel, R , and the bulk temperature T_{Bulk} into (13) gives (14).

$$T_{Bulk} = -\frac{q}{6k_{av}} R^2 + B \quad (14)$$

This allows the second integration constant, B , to be determined.

$$B = T_{Bulk} + \frac{q}{6k_{av}} R^2 \quad (15)$$

Substituting (15) back into (13) gives (16)

$$T = -\frac{q}{6k_{av}} r^2 + T_{Bulk} + \frac{q}{6k_{av}} R^2 \quad (16)$$

And so, the temperature profile within the kernel becomes (17).

$$T = T_{Bulk} + \frac{q}{6k_{av}} (R^2 - r^2) \quad (17)$$

3 Results & Discussion

3.1 Appropriateness of the Cylindrical Approximation

In previous work, a 2D(r - θ) slice through a cylindrical pellet waist or section of cladding was used as an approximation, normally under plane strain, to a 3D cylinder [39, 45, 46, 64, 75]. In this work, a 2D(r - θ) model is used to approximate a 3D sphere. The validity of this approximation therefore needs to be justified.

Figure 4 shows the radial displacement and stress components across the radius of the fuel kernel for the 3D and 2D(r - θ) finite element models of the uniformly heated fuel kernel described in Section 0. Figure 4(a) shows a close agreement between the radial displacement of the plane stress and 3D model, whilst the radial displacement in the plane strain model is 31% greater than the other models. Given that the radial displacement of the kernel-buffer interface is a major driver of stress in the outer layers, the plane stress model appears much more appropriate than the plane strain model as a 2D surrogate. This is reinforced by the compressive out-of-plane stress in excess of 1 GPa in the plane strain model, (shown in Figure 4(b)). This is several orders of magnitude greater than the ± 20 MPa hoop stress across the radius of the kernel in the 3D model shown in Figure 4(c). Comparing the hoop stress in the plane stress and 3D models reveals a similar trend but with a difference in the magnitude. For instance, at the kernel core, the hoop stress predicted by the 3D model is -24 MPa in the 3D model and -10 MPa in the plane stress model. On the outer surface, the values are 24 and 20 MPa respectively. The under-estimate of the stress components in the plane stress model is repeated for the radial stress, as shown in Figure 4(d). The radial stress at the centre of the kernel is -10 MPa in the plane stress model and -24 MPa in the 3D model. Finally, it should be noted that all the stresses predicted for both the 3D and plane stress models are far lower than the 150 MPa fracture stress for the kernel (shown in Table 4).

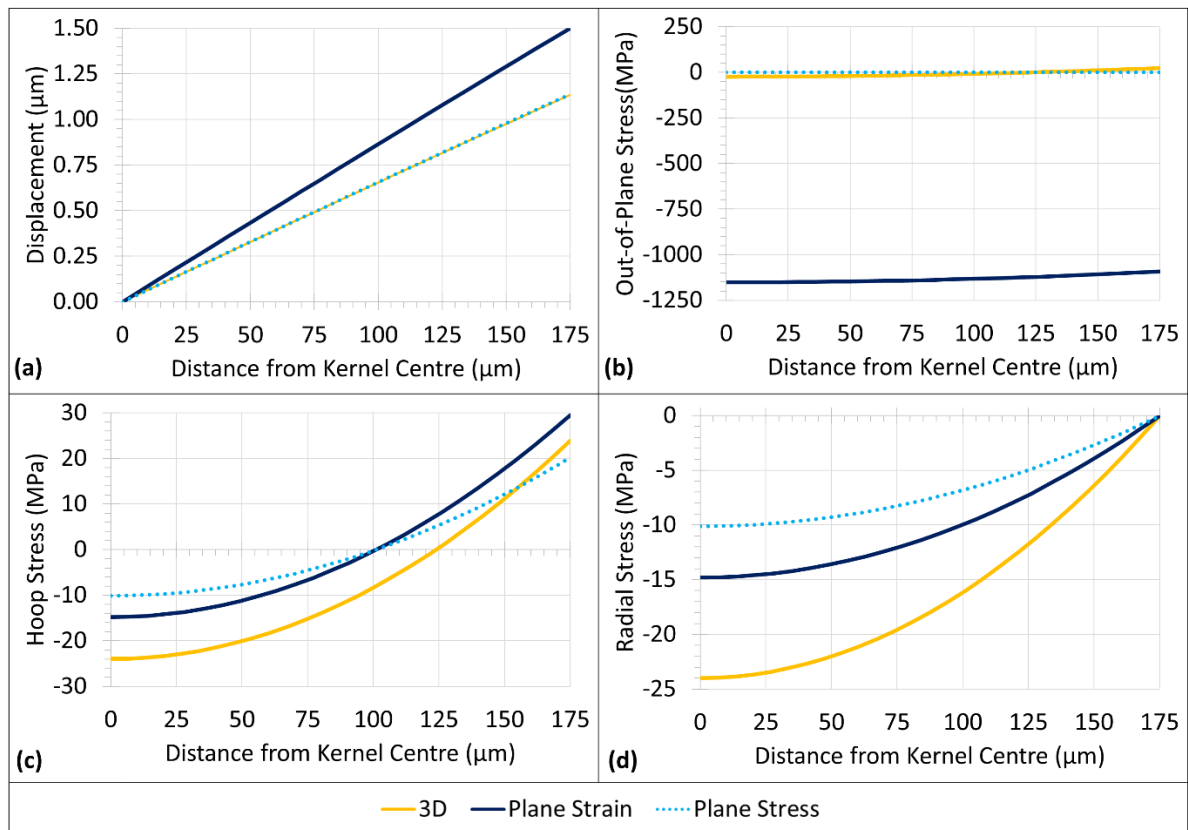


Figure 4 – The radial displacement and stress components across the radius of the fuel kernel for the 3D and 2D(r - θ) finite element models using the separate subroutine detailed in Section 2.4.

3.2 Behaviour of TRISO Particles During Idealised Power Histories

Rise to 100% Power

The temperature profile in the fuel at the end of the rise to power is shown in Figure 5. The temperature drop across the kernel of 18 K is much lower than seen across the pellets of conventional LWR fuel at the start of life, which is approximately 550 K [69]. The temperature gradient is however similar, at 100 K mm⁻¹, compared to the typical gradient of 140 K mm⁻¹ seen in conventional LWR fuel at the same point

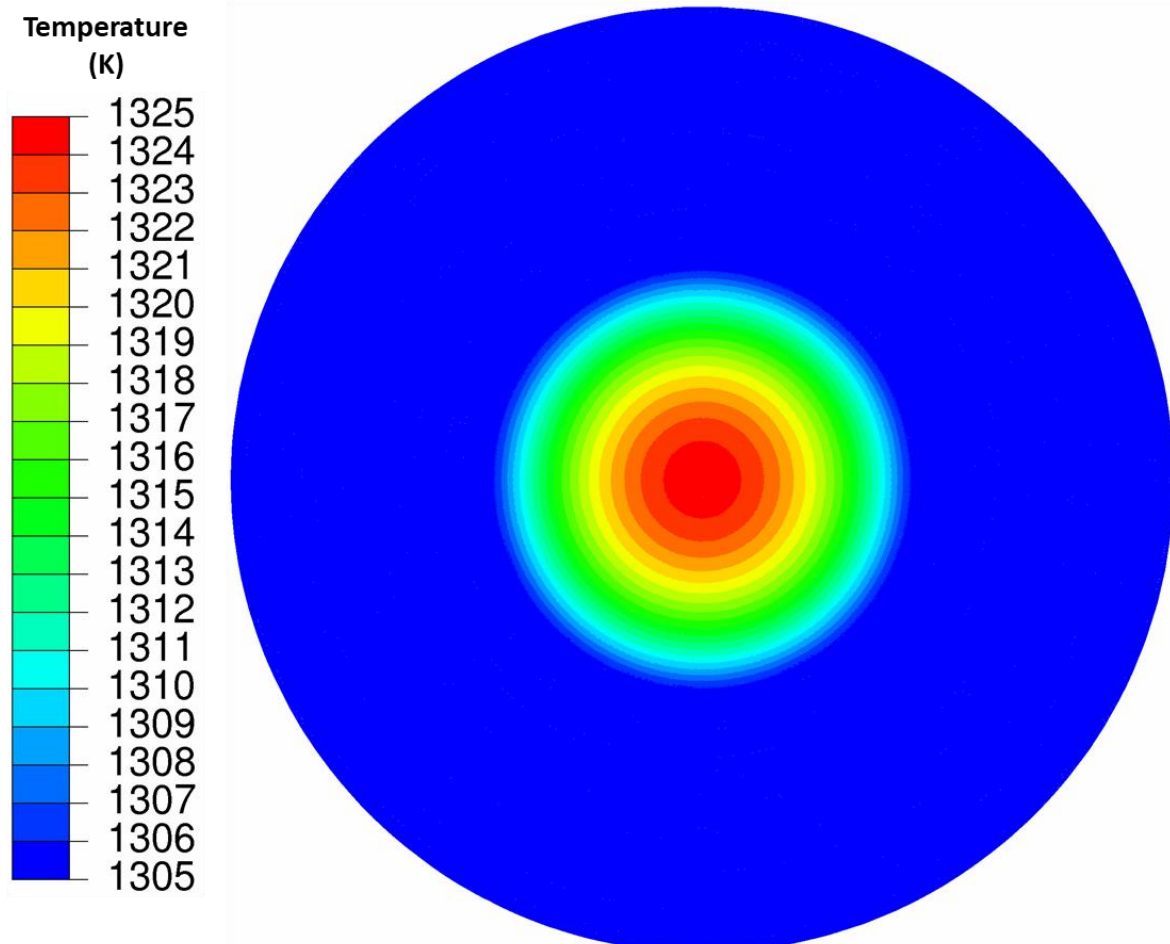


Figure 5 – The temperature in the TRISO particle at the end of the rise to 100% power over 24 hours

Figure 6 shows the fracture pattern in the TRISO particle at the end of a rise to 100% power i.e. normal operation (a kernel power of 0.267 W and a temperature of 1305 K, as described in Section 2.4) over 24 hours. Twenty cracks initiate in the buffer, close to the kernel-buffer interface and around half of these extend outwards radially. They do not however initiate damage in the over-lying iPyC or any of the other layers further towards the outer surface. In addition, circumferential damage is seen in the buffer, close to the kernel-buffer interface. Here, a fundamental difference is seen between TRISO and conventional LWR during the initial rise to power. Namely, that the UO_2 was not predicted to crack in the TRISO fuel, whilst it does in conventional LWR fuel [76]. This might offer potential thermal and fission gas release benefits.

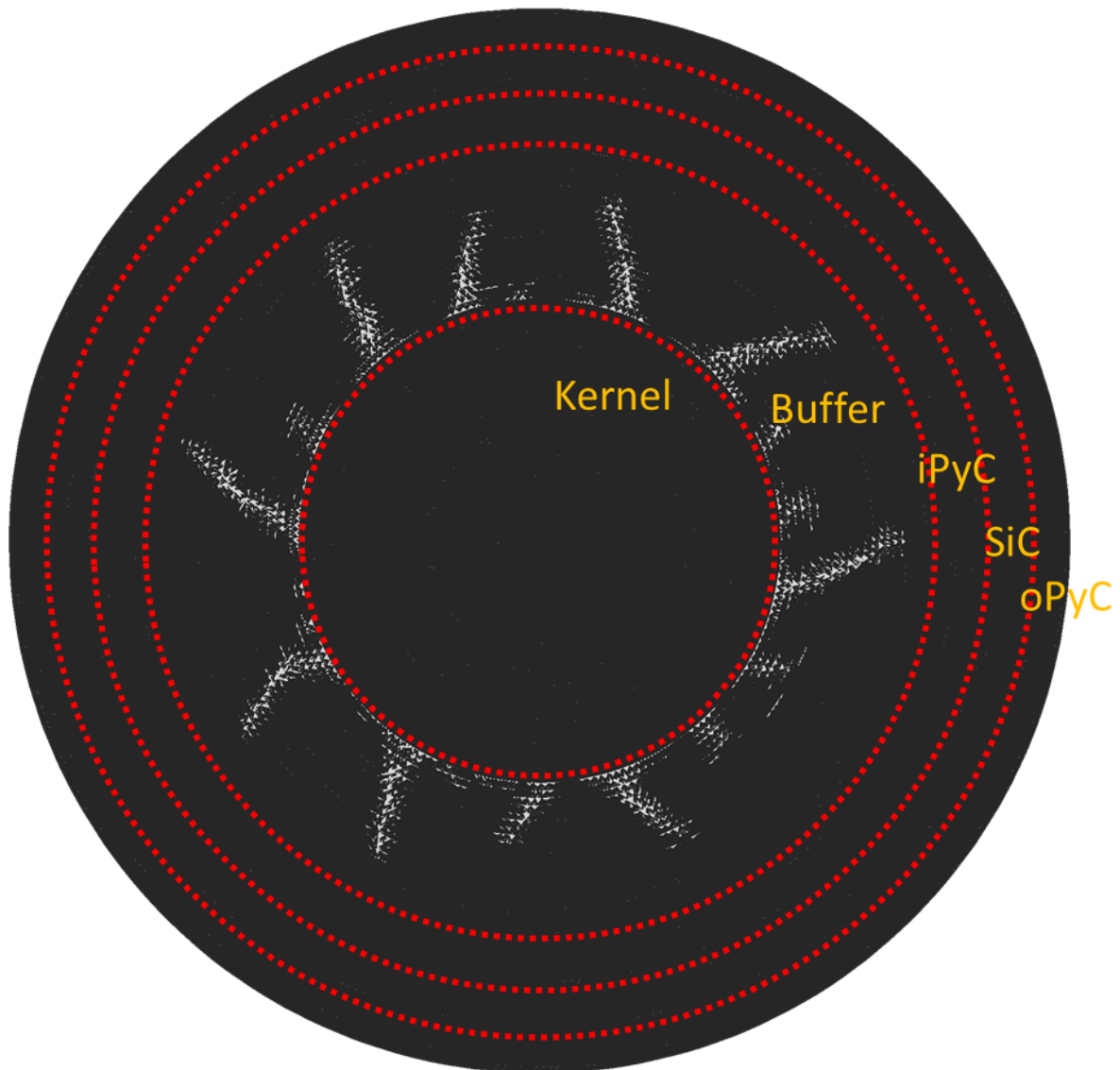


Figure 6 – Fracture patterns in the TRISO particle at the end of the rise to 100% power over 24 hours. Red lines define the layer boundaries and white denotes bond failure, a surrogate for damage / cracking.

Figure 7 shows the percentage power at the end of each increment and demonstrates one of the advantages of implementing bond-based peridynamics in Abaqus. Namely, that explicit time steps can be used during periods of rapid crack propagation and implicit time steps in between. The average time increment during the simulation was 37 s, the minimum 4.3 ns and the maximum 1.8 hours. The simulation took 9.5 hours to run on a Dell Precision 7920 Tower workstation computer with two Intel(R) Xeon(R) Gold 5218R CPU @ 2.10GHz processors running Red Hat Enterprise Linux Server 7.9 and using Intel(R) Fortran version 19.1.3.304 and Abaqus 2020.

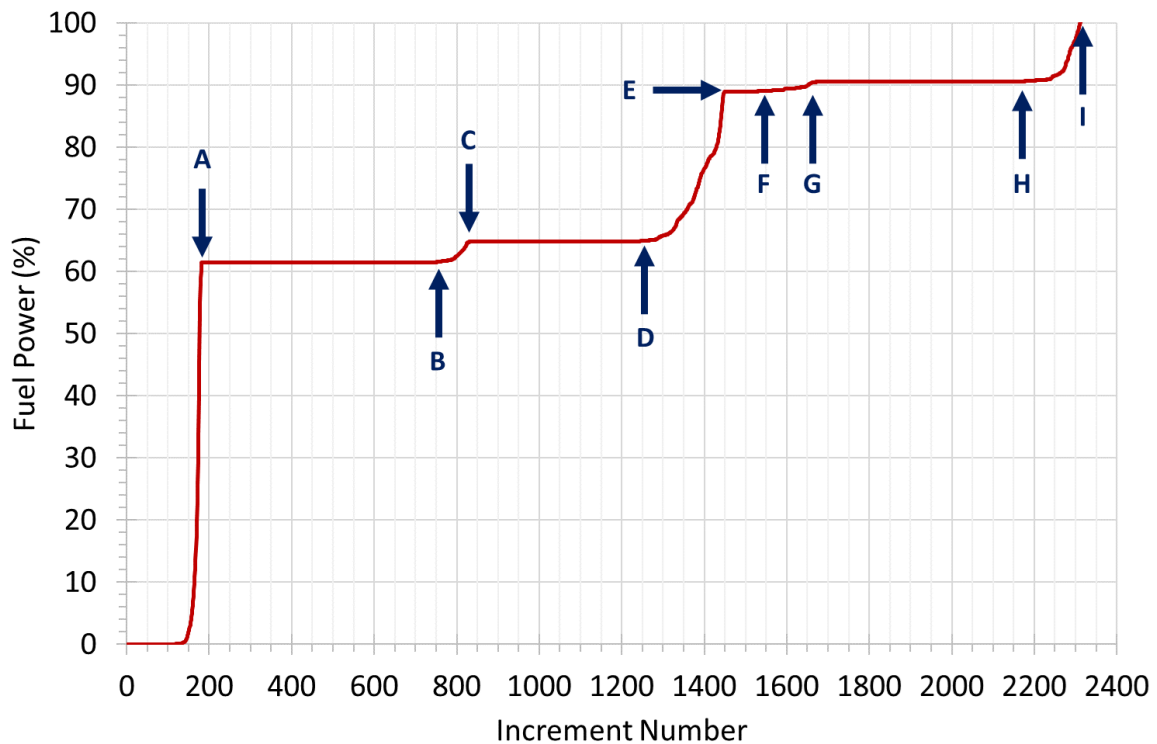


Figure 7 – Incrementation during the simulated rise to 100% power (0.267 W kernel power) over 24 hours. Increment duration ranged from 4.3 ns to 1.8 hours. The letters A-I are points of interest, used in Figure 8.

Figure 8 shows the development of cracking in the buffer at a number of time points indicated in Figure 7. Between 62 and 65% power, there is a period of crack initiation at the kernel-buffer interface (points A to D). This is followed by a period of slow crack growth towards the buffer-iPyC interface (points D to E) until 89-91% power, when additional cracks initiate at the kernel-buffer interface (points E to H). This second period of initiation is followed by a period of slow crack growth towards the buffer-iPyC interface in a smaller subset of cracks (points H to I).

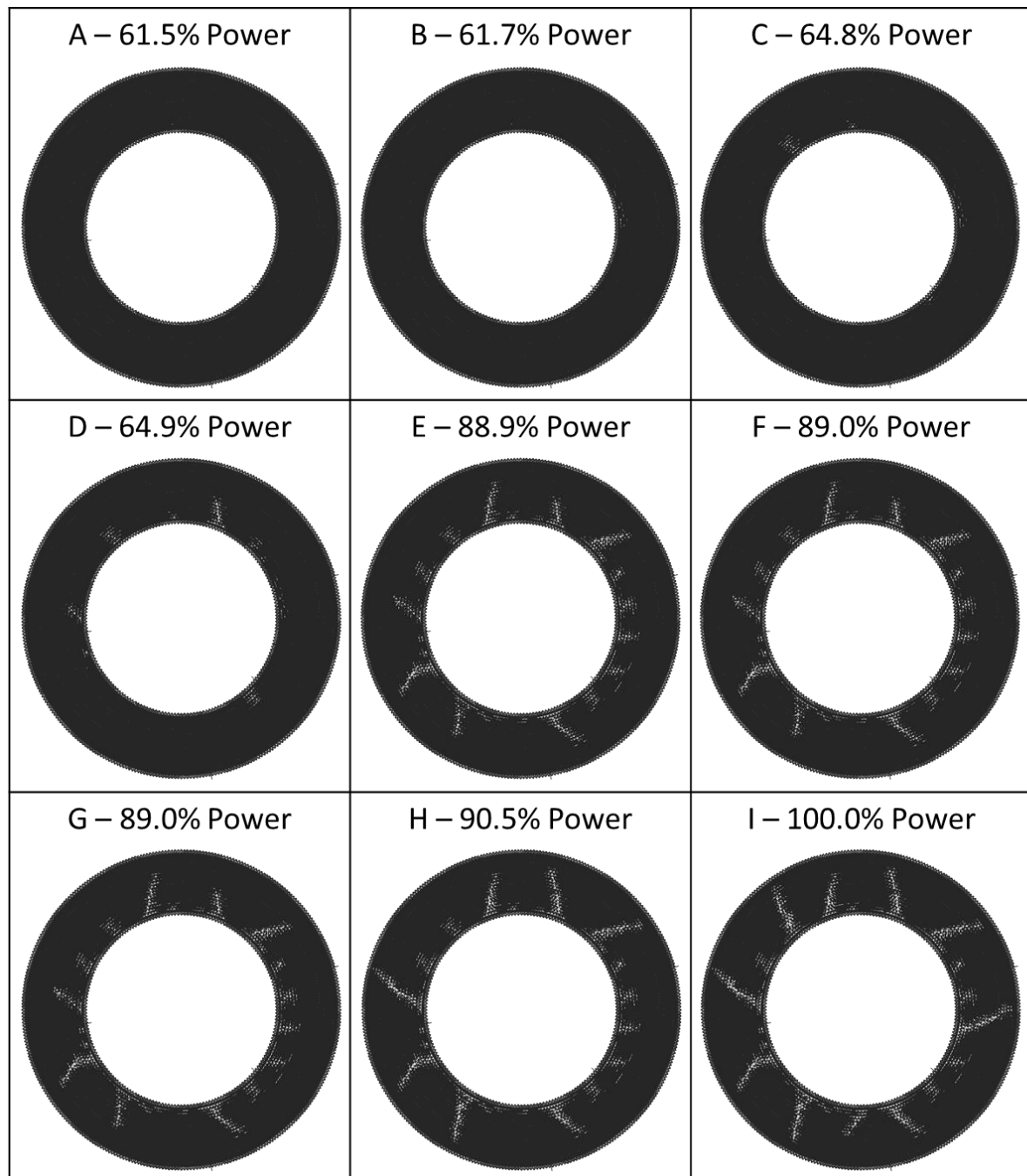


Figure 8 – Crack formation during the rise to full power. The letters A-I are points of interest shown in Figure 7. For clarity, only the buffer region is shown.

Power Ramp from 100% Power

Figure 9 shows the power level reached during the hypothetical extreme power ramp to 1000% power by increment number. In contrast to Figure 7, there are no intermediate stages of periods of rapid cracking, merely the onset of rapid crack growth at 940% power. This high tolerance to a rapid power ramp confirms a potential safety advantage of TRISO particle fuel.

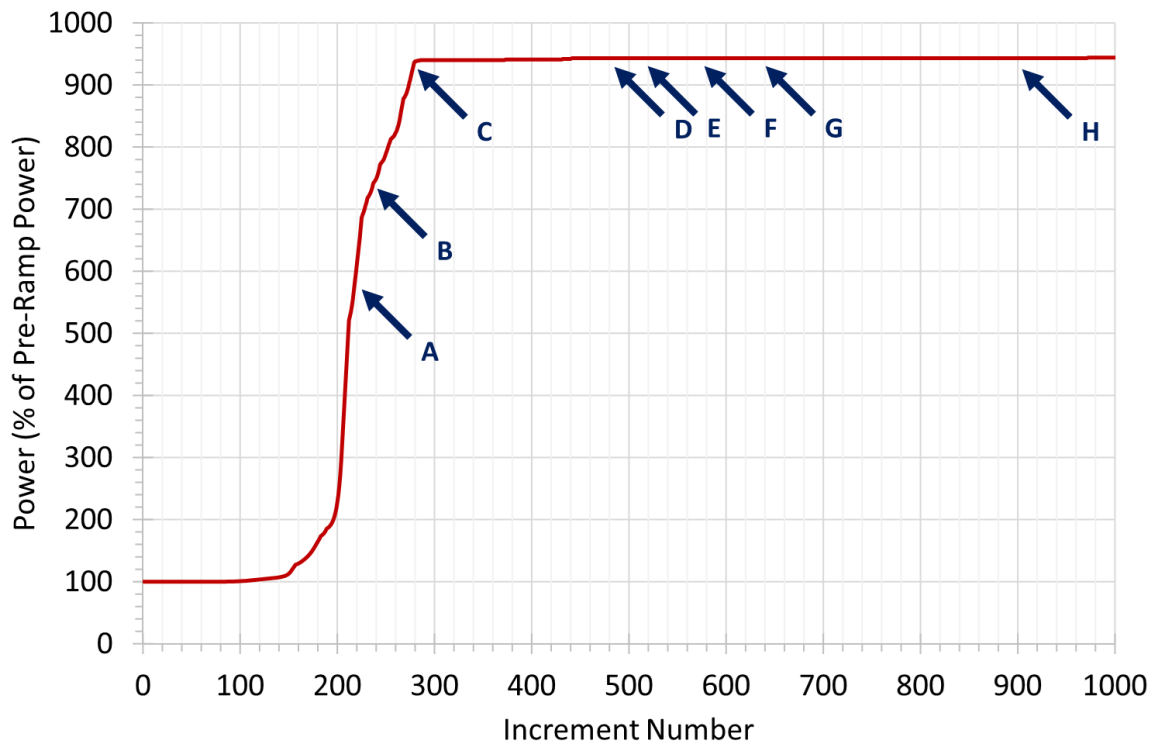


Figure 9 – Incrementation during the simulated power ramp from 100% to 1000% power. Crack patterns at points A to H are shown in Figure 10.

Figure 10 shows the crack patterns at the points A to H shown in Figure 9. At 610% of full power (point A), cracks initiate in the fuel kernel, close to the kernel-buffer interface. These cracks initiate opposite existing cracks in the overlaying buffer. The cracks in the kernel grow slowly (points A to C) until 940% power (point D), when cracks initiate in the SiC at the SiC-PyC interface (points D and E). These cracks increase in number (points F and G) and cracking of the TRISO particle proceeds rapidly towards the outer surface of the SiC layer (point H). It should be noted at point F, the iPyC layer is breached, allowing potential chemical attack of the SiC ‘pressure vessel’ by fission products. In addition, at point H, the SiC pressure vessel is breached, allowing the egress of fission products, especially gases, from the particle.

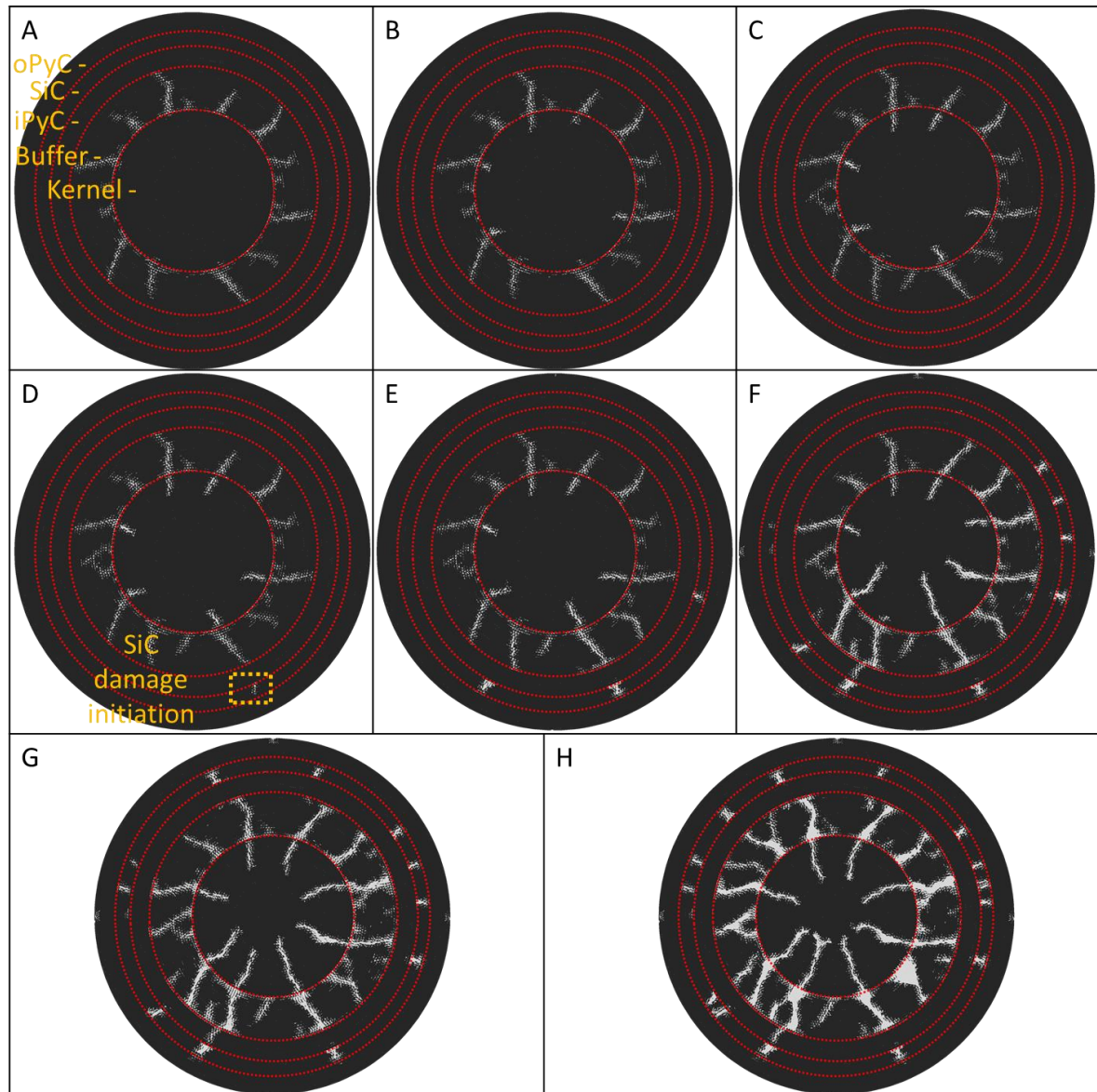


Figure 10 – Crack patterns at the points A to H in the rapid power ramp to 1000% power shown in Figure 9.

Debonding

In this work, we have assumed that the kernel and buffer were initially bonded. There is however evidence that immediately following manufacture, the kernel and buffer are debonded and models treat the interface as being a gap equivalent to the pellet-cladding gap in conventional nuclear fuel [77]. Figure 11(a) is an optical micrograph shows debonding between the buffer and a ZrO_2 kernel manufactured from zirconia, a common surrogate for UO_2 . The clean debonding seen experimentally can be reproduced by our model, as shown in Figure 11(b), which shows clean cracking between the buffer and kernel due to a uniaxial load applied in the horizontal direction. The branching crack is likely to be due to post-initiation twisting leading to increasingly mixed mode loading as the crack grows. The impact of residual stresses due to manufacture and the associated cracking of the kernel-buffer interface is clearly something which deserves further research.

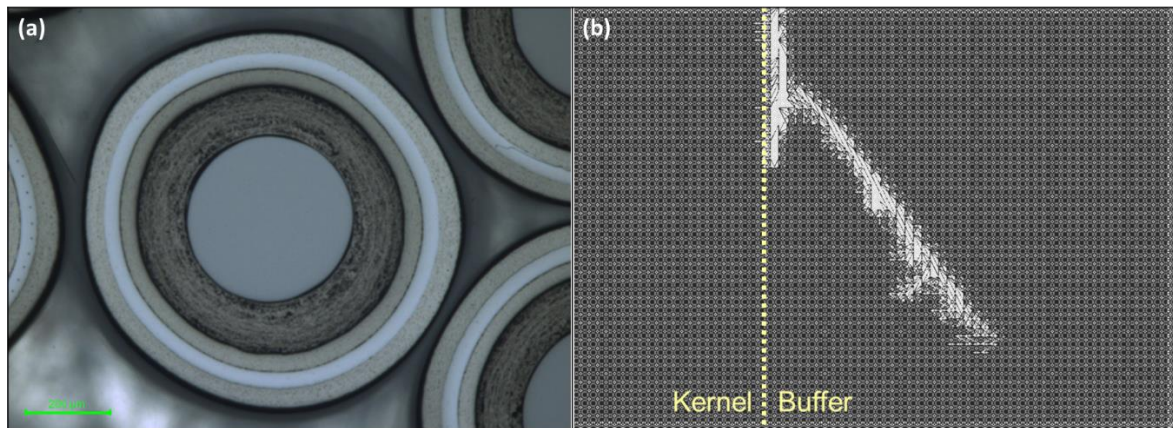


Figure 11 – (a) - An optical micrograph shows debonding between the buffer and a kernel of zirconia. (b) - Cracking between the buffer and kernel due to a uniaxial load applied in the horizontal direction.

If the buffer and kernel are de-bonded, the stress concentration in the kernel might not be as large and so the crack might not ‘jump’ from one material to the other. This in turn, might reduce the stress concentration in the SiC, again analogous to the situation observed in conventional pellet-clad interaction [78].

The formation of cracks in SiC opposite those in the underlying iPyC show the value of employing more advanced explicit crack modelling techniques to predict the failure of TRISO particle fuel than those which do not take into cracks in the underlying layers. The necessity to model cracks in underlying layers is likely to result from the relatively thin nature of the coating layers in a TRISO fuel particle.

4 Conclusions

In this work, we have developed a 2D linear-elastic peridynamic model for TRISO particle fuel during the initial rise to power. This has shown that:

- The most appropriate 2D approximation to the 3D solution for a volumetrically heated sphere is plane stress.
- During an idealised raise to power for a fuel kernel power of 0.267 W and a bulk fuel temperature of 1305 K, cracks initiate in the buffer near to the kernel-buffer interface and propagate radially outwards towards the buffer-iPyC interface. The cracks do not fully penetrate the buffer layer during normal operation.
- During a hypothetical accident involving a power ramp from 100% power (0.267 W) at 0.267 W s^{-1} , cracks formed on the kernel side of the kernel-buffer interface at 610% power. These were opposite existing cracks in the buffer. The cracks in the kernel then propagated slowly.
- The TRISO particle failed at a power of 940%, with numerous cracks rapidly formed at the iPyC-SiC interface, propagating in both directions. During this hypothetical accident, these would overcome the containment to fission gas release offered by the SiC 'pressure vessel'. However, this very high resistance to an extreme power ramp compared to other fuel forms, confirms the potential inherent accident tolerance of coated particle fuel.

Acknowledgements

The authors acknowledge financial support from the UK's Advanced Fuel Cycle Programme (AFCP), funded by the government Department of Business, Energy and Industrial Strategy.

References

- [1] W. Li and K. Shirvan, "ABAQUS analysis of the SiC cladding fuel rod behavior under PWR normal operation conditions," *Journal of Nuclear Materials*, vol. 515, pp. 14-27, 2019, doi: 10.1016/j.jnucmat.2018.12.017.
- [2] Y. He, K. Shirvan, Y. Wu, and G. Su, "Integrating a multi-layer deformation model in FRAPTRAN for accident Tolerant fuel analysis," *Annals of Nuclear Energy*, vol. 133, pp. 441-454, 2019.
- [3] "State-of-the-Art Report on Light Water Reactor Accident-Tolerant Fuels," *Nuclear Energy Agency - Organisation for Economic Co-operation and Development*, 2018, doi: <https://doi.org/https://doi.org/10.1787/9789264308343-en>.
- [4] M. Wagih, B. Spencer, J. Hales, and K. Shirvan, "Fuel performance of chromium-coated zirconium alloy and silicon carbide accident tolerant fuel claddings," *Annals of Nuclear Energy*, vol. 120, pp. 304-318, 2018, doi: 10.1016/j.anucene.2018.06.001.
- [5] K. A. Terrani, "Accident tolerant fuel cladding development: Promise, status, and challenges," *Journal of Nuclear Materials*, vol. 501, pp. 13-30, 2018.
- [6] T. Koyanagi and Y. Katoh, "Mechanical properties of SiC composites neutron irradiated under light water reactor relevant temperature and dose conditions," *Journal of Nuclear Materials*, vol. 494, pp. 46-54, 2017, doi: 10.1016/j.jnucmat.2017.07.007.
- [7] S. Ray, "Accident-Tolerant Fuel: Enhancing Safety," *Nuclear News*, vol. November 2017, pp. 44-47, 2017.
- [8] V. Angelici Avincola, P. Guenoun, and K. Shirvan, "Mechanical performance of SiC three-layer cladding in PWRs," *Nuclear Engineering and Design*, vol. 310, pp. 280-294, 2016, doi: 10.1016/j.nucengdes.2016.10.008.

- [9] H.-G. Kim, Y.-I. Jung, J.-H. Park, D.-J. Park, Y.-H. Koo, and J.-y. Park, "High temperature steam-oxidation behavior of arc ion plated Cr coatings for accident tolerant fuel claddings," *Surface and Coatings Technology*, vol. 280, pp. 256-259, 2015, doi: 10.1016/j.surfcoat.2015.09.022.
- [10] J. G. Stone, R. Schleicher, C. P. Deck, G. M. Jacobsen, H. E. Khalifa, and C. A. Back, "Stress analysis and probabilistic assessment of multi-layer SiC-based accident tolerant nuclear fuel cladding," *Journal of Nuclear Materials*, vol. 466, pp. 682-697, 2015, doi: 10.1016/j.jnucmat.2015.08.001.
- [11] C. P. Deck *et al.*, "Characterization of SiCeSiC composites for accident tolerant fuel cladding," *Journal of Nuclear Materials*, vol. 466, pp. 667-681, 2015.
- [12] S. J. Zinkle, K. A. Terrani, J. C. Gehin, L. J. Ott, and L. L. Snead, "Accident tolerant fuels for LWRs : A perspective," *Journal of Nuclear Materials*, vol. 448, no. 1-3, pp. 374-379, 2014, doi: 10.1016/j.jnucmat.2013.12.005.
- [13] S. Bragg-Sitton, "Overview of International Activities in Accident Tolerant Fuel Development for Light Water Reactors," *US Department of Energy Presentation*, vol. IAEA Techn, 2014.
- [14] T. Helfer, "Recent improvements of the fuel thermomechanical modelling in the PLEIADES Platform to better simulate accidental transients conditions using the Alcyone fuel performance code," *First Workshop on Research into Nuclear Fuel in Europe and Materials Modeling and Simulation for Nuclear Fuels Workshop Karlsruhe, Germany, November 16th to 18th*, 2015.
- [15] C. Marciulescu and A. Sowder, "Uranium Oxycarbide (UCO) Tristructural Isotropic (TRISO) Coated Particle Fuel Performance," *Electric Power Research Institute*, vol. Topical Report EPRI-AR-1 (NP), 2019.
- [16] R. Li, B. Liu, and K. Verfondern, "The study of irradiation-induced failure behavior for the TRISO-coated fuel particle in HTGR," *Journal of Nuclear Materials*, vol. 516, pp. 214-227, 2019.
- [17] R. L. Seibert, B. C. Jolly, M. Balooch, and D. P. Schappel, "Production and characterization of TRISO fuel particles with multilayered SiC," *Journal of Nuclear Materials*, vol. 515, pp. 215-226, 2019.
- [18] R. Li, B. Liu, and C. Tang, "Modification in the stress calculation of PyC material properties in TRISO fuel particles under irradiation," *Journal of Nuclear Science and Technology*, vol. 54, 7, pp. 752-760, 2017.
- [19] W. F. Skerjanc, J. T. Maki, B. P. Collin, and D. A. Petti, "Evaluation of Design Parameters for TRISO coated Fuel Particles to Establish Manufacturing Critical Limits Using PARFUME," *Journal of Nuclear Materials*, vol. 469, pp. 66-105, 2016.
- [20] T. J. Gerczak, J. D. Hunn, R. A. Lowden, and T. R. Allen, "SiC layer microstructure in AGR-1 and AGR-2 TRISO fuel particles and the influence of its variation on the effective diffusion of key fission products," *Journal of Nuclear Materials*, vol. 480, pp. 257-270, 2016.
- [21] B. C. Davis, "Fracture Strength of the SiC Layer in Triso Coated Fuel Particles," *MSc Thesis, Colorado School of Mines*, 2013.
- [22] T. M. Besmann, D. Shin, and T. B. Lindemer, "Uranium nitride as LWR TRISO fuel: Thermodynamic modeling of U-C-N," *Journal of Nuclear Materials*, vol. 427, pp. 162-168, 2012.
- [23] J. J. Powers and B. D. Wirth, "A review of TRISO fuel performance models," *Journal of Nuclear Materials*, vol. 405, pp. 74-82, 2010.
- [24] P. DeMange, J. Marian, M. Caro, and A. Caro, "TRISO-fuel element thermo-mechanical performance modeling for the hybrid LIFE engine with Pu fuel blanket," *Journal of Nuclear Materials*, vol. 405, pp. 144-155, 2010.

- [25] J. C. Gauthier, G. Brinkmann, B. Copley, and M. Lecomte, "ANTARES: The HTR/VHTR project at Framatome ANP," *Nuclear Engineering & Design*, vol. 236, pp. 526-533, 2006.
- [26] D. A. Petti, J. Buongiorno, J. T. Maki, R. R. Hobbins, and G. K. Miller, "Key differences in the fabrication, irradiation and high temperature accident testing of US and German TRISO-coated particle fuel, and their implications on fuel performance," *Nuclear Engineering & Design*, vol. 222, pp. 281–297, 2003.
- [27] K. Minato, T. Ogawa, K. Fukuda, M. Shimizu, Y. Tayama, and I. Takahashi, "Fission product behavior in Triso-coated UO₂ fuel particles," *Journal of Nuclear Materials*, vol. 208, pp. 266-281, 1994.
- [28] J. W. McMurray, T. B. Lindemer, N. R. Brown, T. J. Reif, R. N. Morris, and J. D. Hunn, "Determining the minimum required uranium carbide content for HTGR UCO fuel kernels," *Annals of Nuclear Energy*, vol. 104, pp. 237–242, 2017.
- [29] R. N. Morris, D. A. Petti, D. A. Powers, and B. E. Boyack, "TRISO-Coated Particle Fuel Phenomenon Identification and Ranking Tables (PIRTs) for Fission Product Transport Due to Manufacturing, Operations, and Accidents," *U.S. Nuclear Regulatory Commission Office of Nuclear Regulatory Research*, vol. NUREG/CR-6844, 2004.
- [30] K. Sawa and K. Minato, "An Investigation of Irradiation Performance of High Burnup HTGR Fuel," *Journal of Nuclear Science and Technology*, vol. 36, no. 9, pp. 781-791, 1999.
- [31] K. Lassmann, "TRANSURANUS: a fuel rod analysis code ready for use," *Journal of Nuclear Materials*, vol. 188, pp. 295-302, 1992, doi: 10.1016/0022-3115(92)90487-6.
- [32] P. A. Jackson, J. A. Turnball, and R. J. White, "Enigma fuel performance code," *Nuclear Energy*, vol. 29, 2, pp. 107-114, 1990.
- [33] G. K. Miller, D. A. Petti, and J. T. Maki, "Development of an Integrated Performance Model for TRISO-Coated Gas Reactor Particle Fuel," *HTR-2002: Conference on high temperature reactors; Petten (Netherlands); 22-24 Apr 2002*, pp. 695-700, 2002.
- [34] G. K. Miller, D. A. Petti, J. T. Maki, and D. L. Knudson, "Current Capabilities of the Fuel Performance Modeling Code PARFUME," *HTR-2004: 2nd International Topical Meeting on High Temperature Reactor Technology, Beijing, China (September 22–24, 2004)*, vol. INEEL/CON--04-02240, 2004.
- [35] B. Baurens, J. Sercombe, C. Riglet-Martial, L. Desgranges, L. Trotignon, and P. Maugis, "3D thermo-chemical–mechanical simulation of power ramps with ALCYONE fuel code," *Journal of Nuclear Materials*, vol. 452, pp. 578-594, 2014.
- [36] R. L. Williamson *et al.*, "Validating the BISON fuel performance code to integral LWR experiments," *Nuclear Engineering and Design*, vol. 301, pp. 232-244, 2016.
- [37] T. A. Haynes, V. Podgurschi, and M. R. Wenman, "The Impact of Azimuthally Asymmetric Carbon Deposition upon Pellet- Clad Mechanical Interaction in Advanced Gas Reactor Fuel," *Journal of Nuclear Materials*, vol. 513, pp. 62-70, 2019.
- [38] S. L. N. Dhulipala *et al.*, "Accelerated statistical failure analysis of multifidelity TRISO fuel models," *Journal of Nuclear Materials*, vol. 563, 2022, Art no. 153604.
- [39] T. A. Haynes, D. Shepherd, and M. R. Wenman, "Preliminary Modelling of Crack Formation and Propagation in SiC / SiC Accident-Tolerant Fuel during Routine Operational Transients using Peridynamics," *Journal of Nuclear Materials*, vol. 540, 2020, Art no. 152369.
- [40] G. Hattori and J. Trevelyan, "A Non-Ordinary State Based Peridynamics Implementation for Anisotropic Materials," *Proceedings of the 25th UKACM Conference on Computational Mechanics, 12 - 13 April 2017, Birmingham, United Kingdom*, pp. 106-109, 2017.

- [41] R. Mella and M. R. Wenman, "Modelling explicit fracture of nuclear fuel pellets using peridynamics," *Journal of Nuclear Materials*, vol. 467, pp. 58-67, 2015, doi: 10.1016/j.jnucmat.2015.08.037.
- [42] Y. Wang, X. Zhou, and M. Kou, "Peridynamic investigation on thermal fracturing behavior of ceramic nuclear fuel pellets under power cycles," *Ceramics International*, vol. 44, pp. 11512-11542, 2018.
- [43] S. Oterkus and E. Madenci, "Peridynamic Modeling of Fuel Pellet Cracking," *Engineering Fracture Mechanics*, vol. 176, pp. 23-37, 2017.
- [44] J. D. Jones, T. A. Haynes, G. Rossiter, and M. R. Wenman, "Application of Weibull Fracture Strength Distributions to Modelling Crack Initiation Behaviour in Nuclear Fuel Pellets Using Peridynamics," *Journal of Nuclear Materials*, 2022, Art no. 154087.
- [45] A. Bamgboye, T. A. Haynes, and M. R. Wenman, "Predicting crack patterns in SiC-based cladding for LWR applications using peridynamics," *Structural Integrity Procedia*, vol. 28, pp. 1520–1535, 2020.
- [46] L. D. Jones, L. J. Vandeperre, T. A. Haynes, and M. R. Wenman, "Modelling of Weibull Distributions in Brittle Solids Using 2-Dimensional Peridynamics," *Structural Integrity Procedia*, vol. 28, pp. 1856–1874, 2020.
- [47] T. A. Haynes and M. R. Wenman, "Development of a Peridynamic Material Model for Accident-Tolerant Silicon Carbide – Silicon Carbide Pressurised Water Reactor Cladding " *Report for the National Nuclear Laboratory, Version 4, June 2019*, 2019.
- [48] R. W. Macek and S. A. Silling, "Peridynamics via finite element analysis," *Finite Elements in Analysis and Design*, vol. 43, no. 15, pp. 1169-1178, 2007, doi: 10.1016/j.finel.2007.08.012.
- [49] R. Beckmann, R. Mella, and M. R. Wenman, "Mesh and timestep sensitivity of fracture from thermal strains using peridynamics implemented in Abaqus," *Computer Methods in Applied Mechanics and Engineering*, vol. 263, pp. 71-80, 2013, doi: 10.1016/j.cma.2013.05.001.
- [50] B. Kilic and E. Madenci, "Coupling of peridynamic theory and the finite element method," *Journal of Mechanics of Materials and Structures*, vol. 5, no. 5, pp. 707-733, 2012.
- [51] Q. V. Le and F. Bobaru, "Surface corrections for peridynamic models in elasticity and fracture," *Computational Mechanics*, vol. 61, no. 4, pp. 499-518, 2018, doi: <https://doi.org/10.1007/s00466-017-1469-1>.
- [52] J. Hu and R. Uddin, "3D Thermal Modeling of TRISO Fuel Coupled with Neutronic Simulation," *International Congress on Advances in Nuclear Power Plants*, vol. LA-UR-10-00442, 2010.
- [53] P. A. Demkowicz, D. A. Petti, K. Sawa, J. T. Maki, and R. R. Hobbins, "TRISO-Coated Particle Fuel Fabrication and Performance," *Comprehensive Nuclear Materials (Second Edition)*, vol. 5, pp. 256-333, 2020.
- [54] L. J. Siefken, E. W. Coryell, E. A. Harvego, and J. K. Hohorst, "MATPRO - A Library of Materials Properties for Light-Water-Reactor Accident Analysis," *Idaho National Engineering and Environmental Laboratory*, 2001.
- [55] D. Petti, P. Martin, M. Phélip, and R. Ballinger, "Development Of Improved Models And Designs For Coated-Particle Gas Reactor Fuels," *Idaho National Engineering and Environmental Laboratory Bechtel BWXT Idaho, LLC*, vol. INEEL/EXT-05-02615, 2004.
- [56] K. H. Park, J. Y. Park, J. H. Park, W. J. Kim, C. H. Jung, and Y. W. Lee, "A Novel Approach to the Porosity Evaluation of Pyrolytic Carbon Layers in TRISO-coated Fuel," *Transactions of the Korean Nuclear Society Spring Meeting. Chuncheon, Korea, May 25-26 2006*, 2006.

- [57] R. L. Coble and W. D. Kingery, "Effect of Porosity on Physical Properties of Sintered Alumina," *Journal of the American Ceramic Society*, vol. 39, no. 387-385, 11, 1956.
- [58] L. L. Snead, T. Nozawa, Y. Katoh, T. S. Byun, S. Kondo, and D. A. Petti, "Handbook of SiC properties for fuel performance modeling," *Journal of Nuclear Materials*, vol. 371, pp. 329-377, 2007.
- [59] Y. D. Ha and F. Bobaru, "Studies of dynamic crack propagation and crack branching with peridynamics," *International Journal of Fracture*, vol. 162, pp. 229–244, 2010.
- [60] Y. H. Bie, Z. M. Liu, H. Yang, and X. Y. Cui, "Abaqus implementation of dual peridynamics for brittle fracture," *Computational Methods in Applied Mechanics and Engineering*, vol. 372, 2020, Art no. 113398.
- [61] R. A. Wolfe and S. F. Kaufman, "Mechanical Properties Of Oxide Fuels," *Bettis Atomic Power Laboratory, U. S. Atomic Energy Commission*, vol. WAPD-TM-587, 1967.
- [62] R. G. Munro, "Elastic Moduli Data for Polycrystalline Oxide Ceramics," *Materials Science and Engineering Laboratory, National Institute of Standards and Technology*, vol. NISTIR 6853, 2002.
- [63] A. K. Sengupta *et al.*, "Some Important Properties of Simulated UO₂ Fuel," *BARC/1999/E/008*, 1999.
- [64] T. A. Haynes, J. H. Shea, J. A. Ball, and M. R. Wenman, "Finite element modelling of pellet-clad interaction during operational transients," *TopFuel 2015 Conference Proceedings - European Nuclear Society*, 2015.
- [65] P. G. Lucuta, H. J. Matzke, and I. J. Hastings, "A pragmatic approach to modelling thermal conductivity of irradiated UO₂ fuel: review and recommendations," *Journal of Nuclear Materials*, vol. 1996, no. 232, 1996.
- [66] P. G. Lucuta and H. J. V. Matzke R.A., "Thermal conductivity of hyperstoichiometric SIMFUEL," *Journal of Nuclear Materials*, vol. 223, pp. 51-60, 1995.
- [67] P. G. Lucuta and H. J. V. Matzke R.A., "Modelling of UO₂-based SIMFUEL thermal conductivity: The effect of the burnup," *Journal of Nuclear Materials*, vol. 217, pp. 279-286, 1994.
- [68] J. H. Harding and D. G. Martin, "A recommendation for the thermal conductivity of UO₂," *Journal of Nuclear Materials*, vol. 166, pp. 223-226, 1989.
- [69] R. L. Williamson, "Enhancing the ABAQUS thermomechanics code to simulate multipellet steady and transient LWR fuel rod behavior," *Journal of Nuclear Materials*, vol. 415, no. 1, pp. 74-83, 2011, doi: 10.1016/j.jnucmat.2011.05.044.
- [70] R. L. Williamson and D. A. Knoll, "Simulating Dynamic Fracture in Oxide Fuel Pellets Using Cohesive Zone Models," *20th International Conference on Structural Mechanics in Reactor Technology (SMiRT 20), Espoo, Finland, August 9-14*, vol. 3, 2009.
- [71] L. D. Jones, L. J. Vandeperre, T. A. Haynes, and M. R. Wenman, "Theory and Application of Weibull Distributions to 1D Peridynamics for Brittle Solids," *Computer Methods in Applied Mechanics and Engineering*, vol. 363, 2020, Art no. 112903.
- [72] W. Weibull, "A Statistical Distribution Function of Wide Applicability," *Journal of Applied Mechanics*, vol. 18, no. 3, pp. 293-297, 1951.
- [73] L. P. Rodríguez García, D. M. Pérez, C. R. G. Hernández, D. E. Milian Lorenzo, and C. A. Brayner de Oliveira Lira, "Development of a Methodology for the Evaluation of the Thermomechanical Behavior of the TRISO Fuel," *2017 International Nuclear Atlantic Conference - INAC 2017, Belo Horizonte, Brazil, 22-27 October 2017*, 2017.
- [74] K. F. Riley, M. P. Hobson, and S. J. Bence, "Mathematical Methods for Physics and Engineering," *Cambridge University Press*, vol. Second Edition, 2002.
- [75] T. A. Haynes, J. A. Ball, and M. R. Wenman, "Modelling the Role of Pellet Relocation in the (r- θ) Plane Upon Pellet-Clad Interaction in Advanced Gas Reactor Fuel," *Nuclear Engineering & Design*, vol. 314, pp. 271-284, 2017.

- [76] M. Oguma, "Cracking and Relocation Behaviour of Nuclear Fuel Pellets During Rise to Power," *Nuclear Engineering and Design*, vol. 76, pp. 35-45, 1983.
- [77] C. Zhang *et al.*, "Multidimensional multiphysics modeling of TRISO particle fuel with SiC/ZrC coating using modified fission gas release model," *Annals of Nuclear Energy*, vol. 145, 2020, Art no. 107599.
- [78] T. A. Haynes, J. A. Ball, J. H. Shea, and M. R. Wenman, "Modelling pellet-clad mechanical interaction during extended reduced power operation in bonded nuclear fuel," *Journal of Nuclear Materials*, vol. 465, pp. 280-292, 2015, doi: 10.1016/j.jnucmat.2015.05.021.